Heat-flow and temperature control in Tian–Calvet microcalorimeters: toward higher detection

limits

Heat-flow and temperature control in Tian–Calvet microcalorimeters: toward higher detection limits

L E Vilchiz-Bravo[1], A Pacheco-Vega[2,3] and B E Handy[4,5]

[1] Facultad de Ingeniería Química, Universidad Autónoma de Yucatán, Mérida, YUC 97203, Mexico
[2] Department of Mechanical Engineering, California State University Los Angeles, Los Angeles, CA 90032, USA
[3] Center for Energy and Sustainability, California State University Los Angeles, Los Angeles, CA 90032, USA
[4] CIEP–Facultad de Ciencias Químicas, Universidad Autónoma de San Luis Potosí, San Luis Potosí, SLP 78210, Mexico

E-mail: handy@uaslp.mx

Abstract
Strategies based on the principle of heat flow and temperature control were implemented, and experimentally tested, to increase the sensitivity of a Tian–Calvet microcalorimeter for measuring heats of adsorption. Here, both heat-flow and temperature control schemes were explored to diminish heater-induced thermal variations within the heat sink element, hence obtaining less noise in the baseline signal. PID controllers were implemented within a closed-loop system to perform the control actions in a calorimetric setup. The experimental results demonstrate that the heat flow control strategy provided a better baseline stability when compared to the temperature control. The effects on the results stemming from the type of power supply used were also investigated.

Nomenclature

e	error signal
k_D^Q, k_I^Q, k_P^Q	PID controller gains for the HFC-SHT scheme
k_D^T, k_I^T, k_P^T	PID controller gains for the CTC-T1 scheme
Q	heat flow rate (W)
T	temperature (K)
t	time (s)
u	input voltage signal (V)

Greek symbols

δt	time interval (s)

Subscripts and superscripts

set	setpoint

Abbreviations

CDC	continuously modulated direct current
CTC	conventional temperature control
DAQ	data acquisition
DC	direct current
HFC	heat flow control
PC	personal computer
PID	proportional-integral-derivative
SHT	heat-flow sensor
SP	sample sensing cup
T1	error signal
T2	thermocouple close to SHT
TC	Tian–Calvet
SISO	single-input single-output

[5] Author to whom any correspondence should be addressed.

SSR   solid-state relay
VDC   direct-current voltage

1. Introduction

Amongst the three main types of existing calorimeters, i.e. isothermal, adiabatic and heat flow [1–3], the Tian–Calvet (TC) calorimeter design, based on the heat conduction principle, has been particularly useful in the area of catalysis for studying relatively slow thermal processes associated with gas adsorption [4–7]. From measured heats of adsorption, for instance, it has been possible to characterize the thermodynamic properties associated with different aspects of the catalytic activity of a catalyst surface [8–10]. At the core of a TC calorimeter, the unknown heat flow from a sample volume is directly measured by heat-flux transducers, i.e. differential-temperature sensors, located between the sample holder and a heat sink ideally held at constant temperature. Integration of thermal power versus time then gives the energy emitted during the thermal process. To avoid baseline shifts and signal drift due to external thermal noise, measurements from the sample cell are usually subtracted from those of a reference cell. Additional details of the performance of TC calorimeters can be found in [4, 11, 12].

Design aspects of Tian–Calvet microcalorimeters for gas/solid adsorption studies have been detailed by Parillo and Gorte [11]. Aside from the physicochemical experimental aspects that must be considered in selecting adsorption temperature, they highlight the necessity of insuring that heat and mass transfer rates from the powdered bed to thermopile sensing walls are sufficiently rapid to ensure that adsorption equilibrium is achieved during dosing and throughout the entire sample bed. Importantly, radiative heat losses to surfaces lacking a sensing transducer (i.e. the cell top) can be virtually eliminated by the use of a top layer of chemically inert quartz chips. Radiative heat transfer is operative during the initial gas doses when residual gas pressures in the sample cell are <10 Pa, and can lead to an appreciable thermal shunting away from the sensor walls [13] greater than the 5% uncertainty often reported for these types of experiments. These factors may figure more prominently in high-temperature adsorption calorimetry with oxidation/reduction experiments, where heats of adsorption can be very high ($\geqslant$200 kJ mol^{-1}) and not very reversible.

Accurate prescription of calorimeter sensitivity and detection limits depends heavily on both the instantaneous power level and the duration of experimental heat emission. The limitations in sensitivity and response time have been outlined in [1]. The characteristic time response of the Tian–Calvet calorimeter is slow in comparison to other types, and relates directly, through the Tian equation [4], to the sample cup heat capacity divided by the thermal conductivity of the heat flow transducer wall that surrounds the cup. The calorimeter sensitivity, on the other hand, is a function of the heat flow transducer characteristics and the heat sink stability. Some new calorimeter designs employ more sensitive thermopiles or thermistor elements [14, 15]. But, for a given thermopile geometry and thermo-element characteristics, the sensitivity is limited ultimately by the temperature stability achievable in the heat sink element. This is usually accomplished by employing a sink of sufficiently large thermal mass to minimize temperature gradients. This is a very simple and economical strategy, but may result in a device that is unacceptably large and requires very long stabilization times. Thermal fluctuations in the heat sink element stem from the uneven heat exchange to the ambient air of the laboratory, as well as to power cycling in the heating/cooling systems that are necessary to maintain the heat sink at the desired experimental temperature for studies above or below room temperature. The magnitudes of these noise sources will of course increase with increasing temperature difference between room and experiment.

Of particular interest here is to stabilize high-temperature (i.e. 600 K) calorimetric redox experiments, where the magnitudes of air convective currents and heater power surges are much higher than in calorimetry performed near room temperature. The strategy of using a dual-cup calorimeter design to subtract out spurious non-sample heat signals is effective, although limited by asymmetries in calorimeter geometry and incomplete thermal mass balancing. Inaba *et al* [16] in their analysis of this aspect in a high-temperature calorimeter emphasize the need for the thermal isolation of the heat sink from surroundings, as well as using a sink material with low thermal diffusivity to minimize thermal fluctuations. Other heat sink stabilization strategies employed an inertial temperature control strategy [17] or use Peltier elements as dynamic compensators along with a typical feed-back temperature control [18]. Here we explore the implementation of a heat flow control (HFC) strategy, similar to the one described by Hemmerich *et al* [19] as 'differential temperature control,' as an alternative to directly controlling the temperature at the calorimeter core. In HFC, the control variable is the sensed heat flow, using a thermopile transducer located in close proximity to the heat sink heater element. A particular advantage of this implementation would be to control more effectively the power surges emanating from the heater to heat sink, resulting in smaller fluctuations in the sample cup baseline signal. Traditionally, temperature is the controlled variable as it must normally be maintained to close tolerances in isothermal calorimetry. Yet with heat flow measurements being central to TC calorimetry, it may be desirable to relax these tolerances in order to achieve a reduction in thermal noise at the sample cup heat flow measurements.

In this contribution we propose the implementation of feedback control strategies based on sensing temperature or direct heat flow measurements in order to meet two important operational goals in experiments with TC calorimeters, namely to maintain a particular calorimeter core temperature and to attain lower detection limits by minimizing the baseline heat flow fluctuations in the sample cups. The control strategies are based on the popular proportional-integral-derivative (PID) controller. System dynamics and the signal noise level under temperature-control and heat-flow control are assessed. Additionally, two different power modulation methods (ON/OFF time proportional, and continuous DC
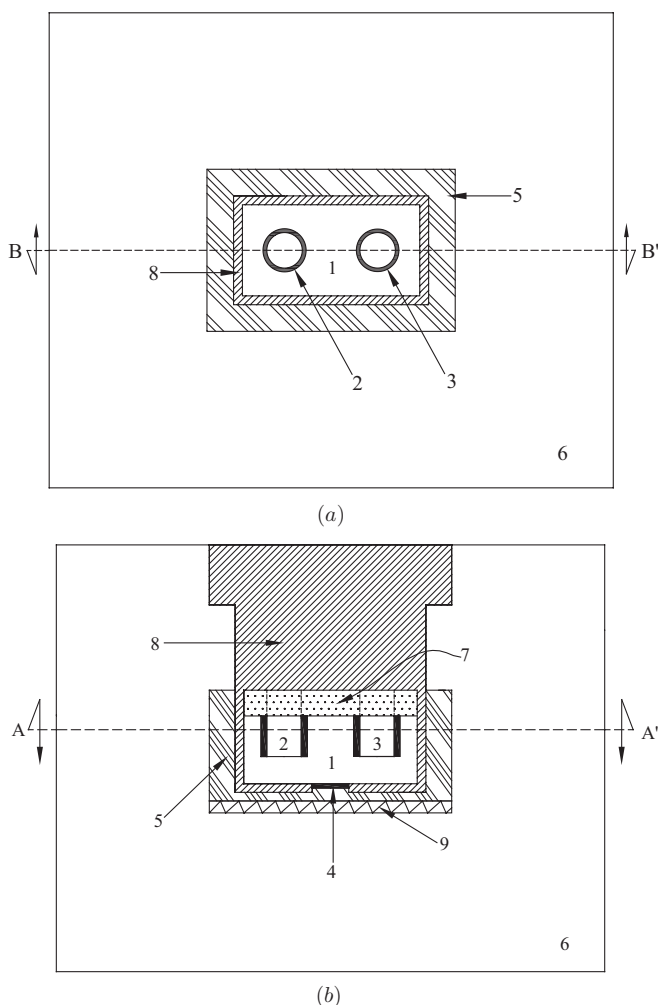
Figure 1. Schematic of a Tian–Calvet microcalorimeter: 1: heat sink, 2: reference-cell sensor, 3: sample-cell sensor, 4: heat flux sensor (HT-50A), 5: stainless steel box, 6: brick-based insulation, 7: ceramic block insulation, 8: fiber glass insulation, 9: electric heater, (*a*) view of section A–A′, (*b*) view of section B–B′.

power modulation) were compared for lowering heat flow noise levels while maintaining a particular core temperature.

2. The Tian–Calvet microcalorimeter system

2.1. Description

The calorimeter used in this investigation, which was constructed specifically to conduct gas/solid adsorption experiments at temperatures exceeding 600 K, is shown schematically in figures 1(*a*) and (*b*). The instrument consists of an outer shell (5), built from stainless steel 304, that is nested with a variety of insulation materials (6, 7 and 8) to dampen temperature variation from external environmental changes. An inner core consists of a pure nickel block (1) which serves as a heat sink for sample heat emissions coming from a dual-cup sensor unit (International Thermal Instruments Co., Del Mar, CA, USA) to measure heat flow signals from quartz-based 1 mm wall, 16 mm diameter × 20 mm height cylindrical sample and reference cells (2, 3)

emitted during a gas adsorption experiment. Output from the sample cup thermopile is designated as 'SP' in the studies described in this work. Two additional sensors were used to provide feedback signals to either the heat-flow- or the temperature-based controllers that are developed here to minimize the fluctuations in the baseline and maintain a quasi-isothermal core temperature. The first sensor (4), designated in text as SHT, was an HT-50 heat flux transducer (ITI Co., Del Mar, CA) placed between the heat sink and the stainless steel box as illustrated in figure 1. The second feedback sensor, designated as T1, is a K-type thermocouple located at the geometrical center of the nickel heat sink, commensurate with maintaining it at the target temperature required for isothermal calorimetry. Energy is supplied to the heat sink through a flat-plate electric heater (9), fastened directly beneath the outer shell component. In order to minimize thermal contact resistance, a good mechanical contact was ensured between the heat sink, the stainless steel shell, SHT, T2 and the underlying heater plate. The amplitude of thermal noise in the sample-cup baseline signal depended upon the heater power supply used. The heater power supply was either of two types: a solid-state relay (SSR) operating in a time-proportional ON–OFF mode or a continuously modulated DC power supply (CDC) that provided smoothly varying DC power levels depending upon the control signal (see the next section).

2.2. Data acquisition system

A diagram of the instrumentation for both data acquisition and control responses in the experimental apparatus is illustrated in figure 2. In this system, information about the heat emitted in the sample cell, the heat sink temperature and the energy supplied to the core unit by the electric heater was first captured by the corresponding sensing elements (i.e. dual-cup thermopiles, thermocouple and heat-flux sensor, respectively), and then collected and processed in a personal computer (PC). A data acquisition (DAQ) card, capable of handling simultaneous measurements up to 16 different channels, provided the corresponding output voltage for the electric heater. The LabVIEW software was used to both interface the experimental system and the controller, and program the PID control law by means of built-in subroutines. Due to the sub-microvolt level readings obtained from thermocouple and thermopile sensors, the analog values were acquired and amplified by two nanovoltmeters (Keithley 2182A) and then sent to the PC via a GPIB card. Measurements of the different variables, in conjunction with their respective sample time, were first acquired by the LabVIEW code and sent to the PID controller program which, in turn, computed the desired control action and returned this information back to the experimental system. Output voltage signals from the controller were processed as follows by the heater power supplies used. In the case of the SSR unit operating in a time-proportional ON–OFF mode, the unit was turned on when the controller output exceeded 1.8 V. With an SSR actuator, the applied 'ON' power, which was determined by a trial and error process, was 134 W. On the other hand, the CDC unit (Xantrex XKW60/50), operated in a constant current mode, provided
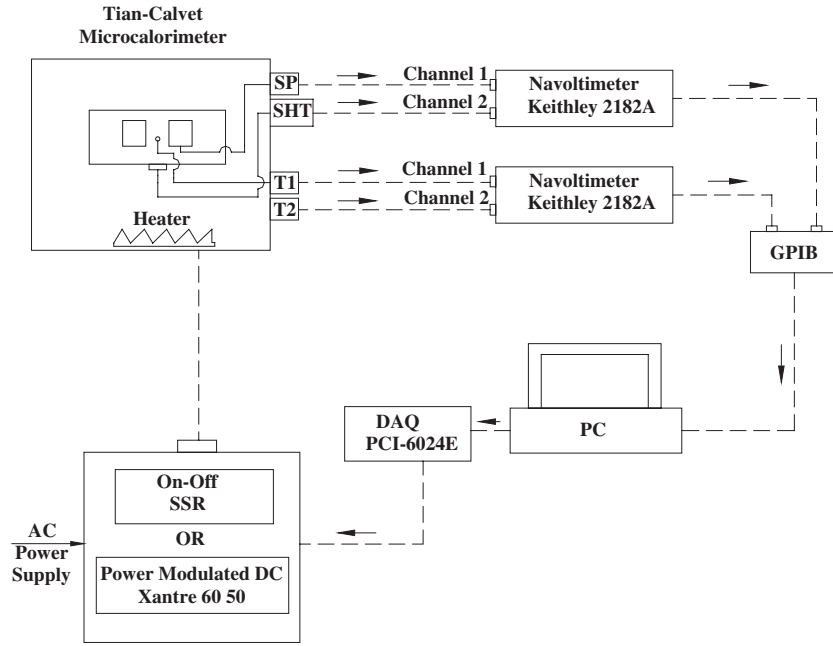
Figure 2. Data acquisition system and control scheme.

filtered DC power levels from 0 to 100% corresponding to the full 0–10 VDC controller output voltage range. The current level was set constant at 4 A, providing a power in the range 0–240 W. Time-dependent information about the generated heat, the core temperature and the heater is finally stored in a data file for later analysis.

3. PID thermal control strategies

The two strategies implemented here are based on PID control loops. These types of controllers are popular in industry due to their simplicity, low cost and adequate response. A main drawback, however, is the necessity for constant attention to achieving optimal performance. Despite this fact, PID controllers are utilized in more than 90% of industrial settings [20]. A PID controller attempts to minimize the difference between measured and desired values in the variables of a process by using a set of control actions: (1) a proportional action to adjust its output according to the size of the error, (2) the integral action that eliminates steady-state offset and (3) the derivative action that provides damping.

3.1. Temperature control

In the conventional temperature control (CTC) strategy, illustrated in figure 3(*a*) as a closed-loop single-input single-output (SISO) system, the goal of the controller is to maintain a specific value of the temperature in the core of the calorimeter. Thus, the electric heater responds to an input signal from the controller, based on the difference between the system output and the setpoint according to the following control law:

$$u_T(t + \delta t) = k_P^T \, e_T(t) + k_I^T \int_{t_0}^{t} e_T(s) \, \mathrm{d}s + k_D^T \frac{\mathrm{d}e_T}{\mathrm{d}t}, \qquad (1)$$
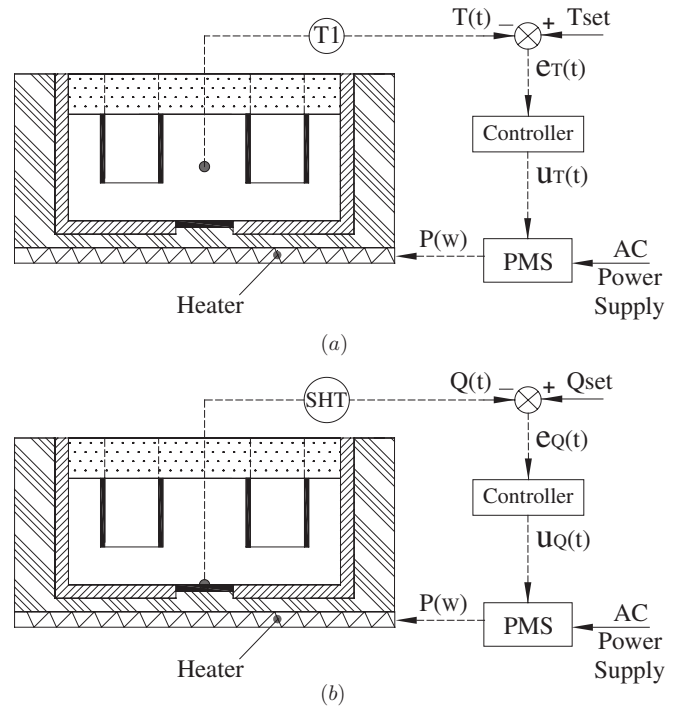

Figure 3. Schematic of closed-loop control strategies. (*a*) Temperature control (CTC-T1). (*b*) Heat flow control (HFC-SHT).

where u_T is the voltage signal to the heater, by means of the power modulated actuator, which takes place at a time δt after the right-hand side of the equation has been evaluated. $e_T(t)$ is the error defined as

$$e_T(t) = T_{\mathrm{set}}(t) - T(t), \qquad (2)$$

with T being the temperature measured by the thermocouple T1 located at the core, as shown in figure 3(*a*), and T_{set} the set point which can either have a fixed value (regulation)

or vary with time (tracking). The parameters k_P^T, k_I^T and k_D^T are the proportional, integral and derivative controller gains, respectively, which were adjusted using a double tuning process with a consecutive application of the Cohen–Coon and Ziegler–Nichols methods [21]. For this type of control strategy the time interval between data acquisition and processing was $\delta t = 1.5$ s. Control experiments using this strategy are designated subsequently as CTC-T1.

3.2. Heat flow control

The heat flow control (HFC) strategy is shown as a closed-loop SISO system in figure 3(*b*). In this case, the objective of the controller is to maintain specific values of the heat flow that is directed toward the core of the calorimeter. The *desired* values, i.e. Q_{set}, are determined *a priori* using direct measurements from the heat-flow sensor (SHT) when the system is under steady-state conditions at the appropriate core temperature T1. The manipulated variable is again the average power level supplied to the electric heater, in accordance with the type of actuator used. The controller output is generated based on

$$u_Q(t + \delta t) = k_P^Q \, e_Q(t) + k_I^Q \int_{t_0}^t e_Q(s) \, \mathrm{d}s + k_D^Q \frac{\mathrm{d}e_Q}{\mathrm{d}t}, \qquad (3)$$

where u_Q is the voltage signal to the heater coming from the controller, via the power modulated actuator, occurring at time $t + \delta t$. The error $e_Q(t)$ is now defined as

$$e_Q(t) = Q_{set}(t) - Q(t), \qquad (4)$$

where Q is the heat flow passing through the SHT sensor located below the calorimeter core, as shown in figure 3(*b*) and Q_{set} is the set point value. As before for the CTC-T1 control scheme, the parameters k_P^Q, k_I^Q and k_D^Q in equation (3) were tuned in a similar way, i.e. using a double tuning process. For the sake of consistency in the experimental tests under the action of either controller, the time interval between data acquisition and processing was also set in this case at $\delta t = 1.5$ s. This control strategy is designated as HFC-SHT in the runs below.

It is to be noted that the aforementioned double-tuning process used for adjusting the parameters of both controllers was based on the natural open-loop dynamic response of the calorimeter system, shown in figure 4, when the amount of power supplied to the heat sink is increased in a step-like manner to increase the value of the core temperature from 557.5 to 582.5 K. Figures 4(*a*) and (*b*) illustrate, respectively, the typical evolution of both temperature and heat flow as sensed by the thermocouple T1 and the heat flow sensor SHT. In figure 4(*a*) it can be easily observed what appears to be the familiar response of a first-order time-dependent system for the temperature at T1, which, from a global energy-balance perspective in the core, suggests a second-order critically damped-type response in the heat flow (energy transfer) signal, as depicted in figure 4(*b*). From the figures it can also be observed that after about 50 h the temperature and heat flow signals have reached their steady-state values. For the control tests shown in the next section, this type of test measurement served as a basis to estimate the heat flow required to maintain a specific core temperature at T1.
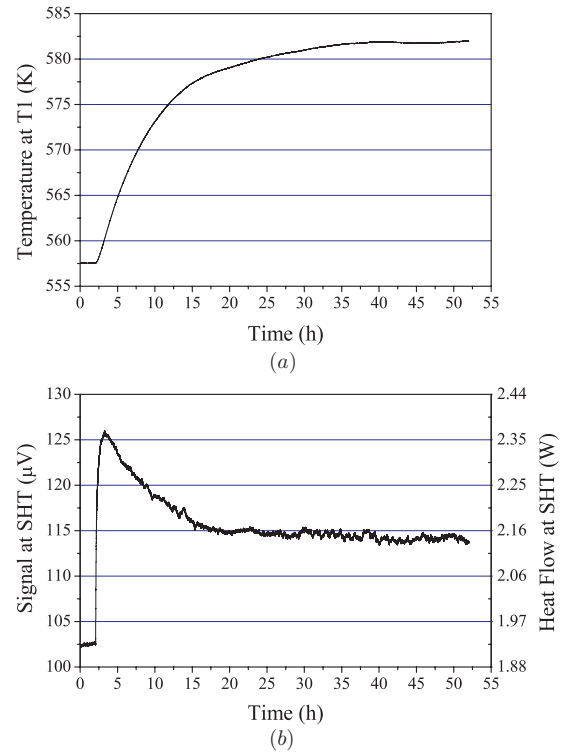

Figure 4. System response due to change in core temperature from 557.5 K to 582.5 K. (*a*) Temperature measured at T1. (*b*) Heat flow measured at SHT.

4. Results and discussion

4.1. Change in the setpoint for temperature and heat flow

In the first series of tests, the evolution in time of the temperature at T1 and of the heat flow measured at SHT were studied under the action of the two different control schemes, using SSR power regulation to modulate the heater power. The corresponding results are shown in figure 5 for two cases: (1) a step-like change in the temperature setpoint and (2) a change in the setpoint of the heat flow rate. For both tests, the temperature traces of T1 versus time are depicted in figure 5(*a*), and the corresponding traces of the heat flow at SHT are given in figure 5(*b*). Prior to introducing the step changes, the system was allowed to reach steady-state over at least a 10 h interval, after which T1 fluctuations were random and equal to 0.1 K.

First using CTC-T1 with tuned PID parameters, the setpoint temperature at T1 was raised 50 K, from 523 K to 573 K. As can be seen, in agreement with the system behavior reported in the previous section, the T1 response is monotonic and establishes the new setpoint value after about 17 h. Heat flow traces show that, in order to reach this new temperature, the CTC-T1 controller acting upon the electric heater overshoots within the first hour after which heat-flow levels decrease toward the new steady-state value in an apparent first-order manner, with noise oscillations reappearing after about 18 h when power-cycling resumes.

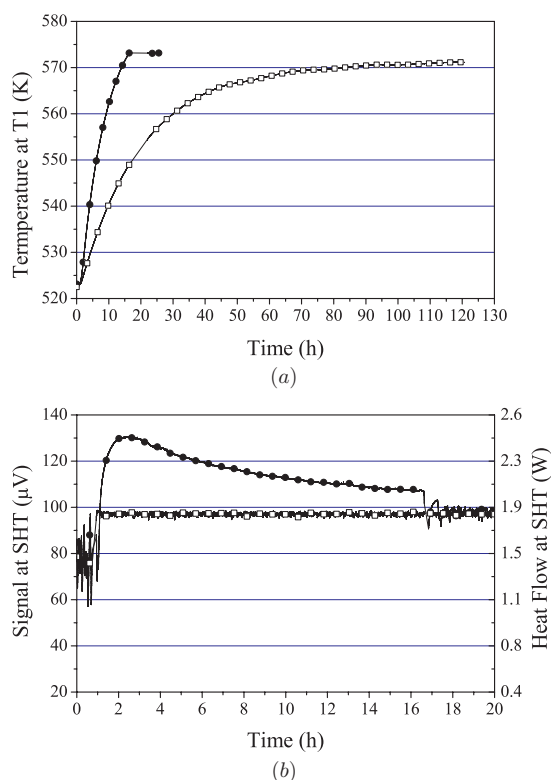With the system under CTC-T1 at steady conditions, the average heat flow signal from SHT registered 76 μV

Figure 5. System response to the application of the different control schemes. (-●-) CTC-T1. (-□-) HFC-SHT. (*a*) Temperature history at T1 location. (*b*) Heat flow history at SHT location.

(1.41 W) with T1 at 523 K and 97 μV (1.85 W) with T1 at 573 K. These voltage-/heat-flow values were then used to establish $Q_{\rm set}$ when switching to heat flow control to observe the T1 response toward the desired temperature setpoint. As can be seen, under HFC-SHT, the T1 response is considerably slower than under CTC-T1, requiring several days to approach the new steady-state temperature level. These circumstances are probed further from the SHT traces showing that, as HFC-SHT controller is able to reach the new setpoint value in the heat flow within the first hour, due to the substantially lower power-level supplied to the core, the amount of time required to provide the energy necessary to take T1 to its pre-established setpoint must be longer than that under the CTC-T1 control. Results from these tests are indicative that simply controlling the heat flow supplied to the calorimeter core may not be sufficient to achieve the practical objective of maintaining the temperature at the core within reasonable precision.

4.2. System response to switchover between CTC-T1 and HFC-SHT schemes

In a separate run, depicted in figure 6, traces of the T1 temperature and heat flows at SHT and SP (the latter being the heat flow signal from one of the sample cup thermopiles) are recorded first at the control setpoint under CTC-T1 action (for $t < 8$ h) with T1 set at 573 K, then switching over to the HFC-SHT control regime (for $t \geqslant 8$ h). Under CTC-T1, heater-induced oscillations are considerably higher in both recorded heat flow traces than in T1, where they are barely resolvable. This can be attributed to power surges during
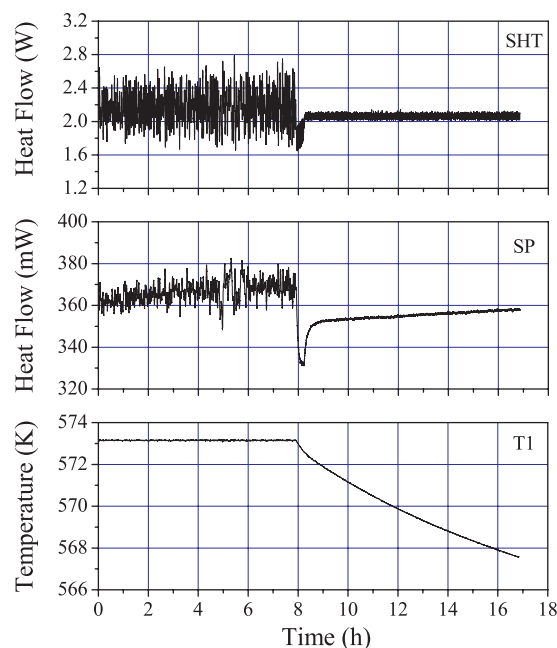

Figure 6. Change in the system response for a switchover from CTC-T1 for $t < 8$ h to HFC-SHT for $t \geqslant 8$ h.

the ON–OFF cycling of the SSR regulator under this control scheme, the surges manifesting themselves most strongly in the sensor (SHT) located close to the heater element. The lower heat flow amplitude in SP and constant level of T1 are due to the damping (averaging) effect of the thermal mass in the heat sink element and, specifically in the case of T1, to the control action from CTC-T1 that takes place to keep the temperature as stable as possible at the setpoint value.

During the switchover to HFC-SHT at $t = 8$ h, the heat flow readings show more rapid stabilization at SHT than at SP, due to the natural thermal lag from the heat sink. This rapid re-adjustment period occurred within the first hour after switchover. The HFC-SHT acting upon the heater to maintain a stable heat-flow value brought about a several-fold noise reduction in all readings. It is to be noted that the temperature readings decline after this point since the newly established setpoint heat flow value was slightly lower than the true steady-state value required to maintain T1 (under CTC-T1) at 573 K. The T1 response is also considerably slower than the SP heat-flow response because of thermal inertia in the core. The prolonged slightly positive drift in SP, however, could not be attributed to the lower setpoint used—one would expect the SP signal to decline with decreasing core temperature while maintaining the heater influx constant. More likely, this is an indication that the calorimeter is increasing its heat losses with the laboratory surroundings, which could be the case if the room temperature decreases.

These observations further suggest a modified control strategy: it may be possible to more rapidly achieve a constant heat sink temperature target value for isothermal experiments, and maintain a constant heat flow baseline (SP) by sampling T1 and SHT simultaneously, incrementally changing the heat flow setpoint such that T1 approaches its desired temperature level.
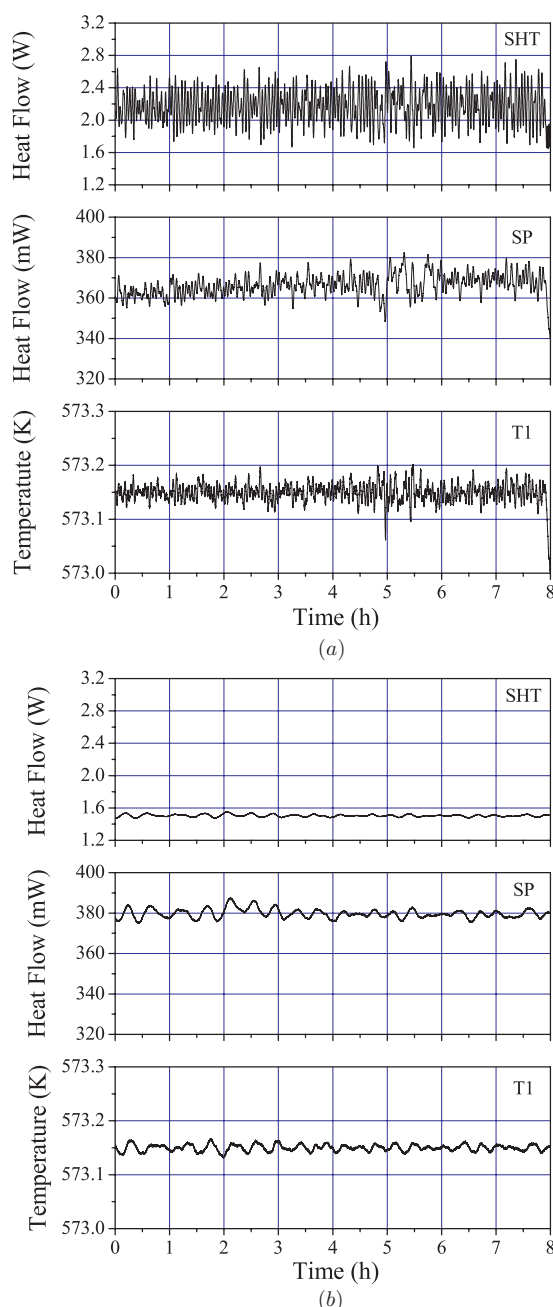
Figure 7. Comparison of the system response under the CTC-T1 scheme for different power-supply systems. (*a*) SSR power supply. (*b*) CDC power supply.

4.3. Effect of the power supply actuator on the system response

Though the application of HFC-SHT allows one order of magnitude reduction in the amplitude of the thermal noise with respect to that obtained under CTC-T1, short-period oscillations are still noticeable, as observed in figure 6. The presence of these variations in the temperature and heat flow measurements appears to be a result from excessive power surging in the SSR supply system, suggesting that a filtered power modulation supply could eliminate them. This effect is explored by means of two experiments, as reported in figure 7. In each test the system is maintained at the

appropriate temperature setpoint under the action of the CTC-T1 controller. The results for the case where the voltage signals to the heater are supplied by the SSR actuator are shown in figure 7(*a*), whereas figure 7(*b*) displays the results for the case where the CDC power supply unit is employed.

From the figures it can be seen that with the SSR power supply, the peak-to-peak noise in T1 and SHT are, in average, 0.06 K and 0.45 W, respectively. The short period (3–4 min) oscillations are entirely eliminated when the CDC unit is employed as the heater power supply, being replaced by longer period fluctuations (about 25 min) with reduced average p–p levels of 0.025 K and 0.05 W in TI and SHT, respectively. Importantly, the baseline noise at the calorimeter sample cup SP is also significantly reduced (from 15 mW to about 5 mW averaged p–p values), although it mirrors the oscillations seen at T1. These longer nearly periodic fluctuations are not due to imperfect tuning of the controller parameters; rather they are due to the presence of thermal lag between the heater and the core temperature location. Elimination of these oscillations is currently under investigation.

The adequate performance of the controller can be further noted from figures 7(*a*) and (*b*), showing that despite the fact that the temperature of the surrounding laboratory space is different between experiments being reported here, the CTC-T1 is able to maintain the core temperature within a range very close to the desired setpoint of 573.15 K. The average values of the heat flow, as sensed at SHT and SP (2.2 W and 365 mW, respectively), which are required to sustain the core temperature at the desired point, are higher under SSR than when the CDC is applied (1.5 W and 380 mW, respectively), implying a lower room temperature during the SSR-based experiment.

The effect of modulated power supply used was also investigated under the HFC-SHT strategy. These results, not shown here, were in very close agreement with the results presented in this section for the CTC-T1 scheme.

5. Conclusions

Experimental tests demonstrate that the use of the heat flow control scheme, compared to the direct control of the calorimeter core temperature, results in nearly one order of magnitude noise reduction in the heat flow baseline noise measured at one of the sample sensing cups. Use of a CDC power supply virtually eliminated short-period power surging that was present when a simpler SSR-based power supply was used in the ON/OFF time-proportional mode. At this point, heater-induced noise is at a minimum, and further thermal noise reduction at the sensing cups can only be achieved by a better control of external (room) variations.

On the other hand, the temperature-based control strategy is most efficient for maintaining an isothermal core. For practical calorimeter operation, these two objectives, although related, are indeed different. It may, therefore, be necessary to further investigate the implementation of a modified control scheme that senses both temperature and heat flow for the purpose of rapidly establishing a target temperature level for isothermal calorimetry and a suitably steady heat flow baseline within the same time period. In this mixed strategy

the parameters of a multi-objective control scheme can be optimized to achieve the overall goal of maintaining a particular calorimeter core temperature and attaining smaller detection limits.

Acknowledgments

References

[1] Hansen L D and Eatough D J 1983 Comparison of the detection limits of microcalorimeters *Thermochim. Acta* **70** 257–68

[2] Wadsö I 2000 Needs for standards in isothermal microcalorimetry *Thermochim. Acta* **347** 73–7

[3] Hansen L D 2001 Toward a standard nomenclature for calorimetry *Thermochim. Acta* **371** 19–22

[4] Gravelle P C 1972 Heat-flow microcalorimetry and its application to heterogeneous catalysis *Adv. Catal.* **22** 191–263

[5] Gravelle P C 1977 Calorimetry in adsorption and heterogeneous catalysis studies *Catal. Rev.—Sci. Eng.* **16** 37–110

[6] Handy B E, Sharma S B, Spiewak B E and Dumesic J A 1993 A Tian–Calvet heat-flux microcalorimeter for measurement of differential heats of adsorption *Meas. Sci. Technol.* **4** 1350–6

[7] Hansen L D 2000 Calorimetric measurement of the kinetics of slow reactions *Ind. Eng. Chem. Res.* **39** 3541–9

[8] Cardona-Martinez N and Dumesic J A 1992 Applications of adsorption microcalorimetry to the study of heterogeneous catalysis *Adv. Catal.* **38** 149–244

[9] Auroux A 2002 Microcalorimetry methods to study the acidity and reactivity of zeolites, pillared clays and mesoporous material *Top. Catal.* **19** 205–13

[10] Hart M P and Brown D R 2004 Surface acidities and catalytic activities of acid-activated clays *J. Mol. Catal. A: Chem.* **212** 315–21

[11] Parrillo D J and Gorte R J 1998 Design parameters for the construction and operation of heat-flow calorimeters *Thermochim. Acta* **312** 125–32

[12] Vilchiz-Bravo L E 2007 Heat transfer numerical simulations and control strategies to improve thermal sensitivity in Tian–Calvet calorimeters (in Spanish) *PhD Thesis* Universidad Autónoma de San Luis Potosí, San Luis Potosí, Mexico

[13] Vilchiz L E, Pacheco-Vega A and Handy B E 2005 Heat-flow patterns in Tian–Calvet microcalorimeters: conductive, convective, and radiative transport in gas dosing experiments *Thermochim. Acta* **439** 110–8

[14] Garcia-Cuello V, Moreno-Pirajan J C, Giraldo-Gutierrez L, Sapag K and Zgrablich G 2008 Design, calibration, and testing of a new Tian–Calvet heat-flow microcalorimeter for measurement of differential heats of adsorption *Instrum. Sci. Technol.* **36** 455–75

[15] Garcia-Cuello V, Moreno-Pirajan J C, Giraldo-Gutierrez L, Sapag K and Zgrablich G 2009 Adsorption micro calorimeter: design and electric calibration *J. Therm. Anal. Calorim.* **97** 711–5

[16] Inaba H, Takahashi S, Mima T and Naito K 1984 A high temperature Tian–Calvet type calorimeter and an analysis of the baseline fluctuation *J. Chem. Thermodyn.* **16** 573–82

[17] Hemmerich J L, Serio L and Milverton P 1994 High-resolution tritium calorimetry based on inertial temperature control *Rev. Sci. Instrum.* **65** 1616–20

[18] Velazquez-Campoy A, Lopez-Mayorga O and Cabrerizo-Vilchez M A 2000 Development of an isothermal titration microcalorimetric system with digital control and dynamic power Peltier compensation: I. Description and basic performance *Rev. Sci. Instrum.* **71** 1824–31

[19] Hemmerich J L, Loos J-C, Miller A and Milverton P 1996 Advances in temperature derivative control and calorimetry *Rev. Sci. Instrum.* **67** 3877–84

[20] Yu C C 1999 *Autotuning of PID Controllers* (London: Springer)

[21] Åström K J and Hägglund T 2005 *Advanced PID Control* (Research Triangle Park, NC: ISA—The Instrumentation, Systems, and Automation Society)